ELSEVIER

Engineering Analysis with Boundary Elements 29 (2005) 494–510

ENGINEERING ANALYSIS *with* BOUNDARY ELEMENTS

www.elsevier.com/locate/enganabound

Generalized boundary element method for galerkin boundary integrals

L.C. Nicolazzi[a,*], C.S. Barcellos[b], E.A. Fancello[a], C.A.M. Duarte[c]

[a]*Departamento de Engenharia Mecânica, Universidade Federal de Santa Catarina, Florianópolis, SC 88010-970, Brazil*
[b]*IPUC, Pontifícia Universidade Católica de Minas Gerais, Belo Horizonte, MG, CEP 30535-610, Brazil*
[c]*Department of Mechanical Engineering, University of Alberta, Edmonton, AB, Canada*

Received 19 April 2004; revised 1 December 2004; accepted 23 December 2004
Available online 22 April 2005

Abstract

A meshless approach to the Boundary Element Method in which only a scattered set of points is used to approximate the solution is presented. Moving Least Square approximations are used to build a Partition of Unity on the boundary and then used to construct, at low cost, trial and test functions for Galerkin approximations. A particular case in which the Partition of Unity is described by linear boundary element meshes, as in the Generalized Finite Element Method, is then presented. This approximation technique is then applied to Galerkin boundary element formulations. Finally, some numerical accuracy and convergence solutions for potential problems are presented for the singular, hypersingular and symmetric approaches.

Keywords: Galerkin method; BEM p-adaptivity; Symmetrical BEM; Hp-Clouds; Partition of unity

1. Introduction

In the last decade a number of meshless procedures have been proposed in the FEM community. These include: The Smoothed Particle Hydrodynamics Method, The Diffuse Element Method [1], Wavelet Galerkin Method [2], The Element Free Galerkin Method, (EFGM), [3], Reproducing Kernel Particle Method (RKPM) [4], The Meshless Local Petrov–Galerkin Method [5], the Natural Element Method [6], Partition of Unity Method [7], and the hp-Cloud Methods e.g. [8,9]. The latter has the further appeal of naturally introducing a procedure for performing hp-adaptivity, in a very flexible way, avoiding the construction of functions by sophisticated hierarchical techniques. The advantages of these procedures are, however, balanced by increased computational cost since a mesh is still needed for integration purposes and, at each integration point, the Partition of Unity must be computed since the covering of each point is arbitrary. The cost can be reduced by using a linear Lagrangian Partition of Unity as in the Finite Element Method as proposed by Oden, Duarte and Zienkiewicz [10] and later denoted by the Generalized Finite Element Method [11], (GFEM), which can be understood as a Generalization of the Partition of Unity Method [7]. More recently, Sukumar and his co-workers [12], proposed the Extended Finite Element Method, (XFEM), which presents similar characteristics as the GFEM.

The meshless procedures have also attracted the attention of an increasing number of researchers within the Boundary Element community. Among many contributions, we may cite the Boundary Node Method [13–15], Local Boundary Integral Equation [16,17], Boundary Particle Method [18], Radial Point Interpolation Meshless Method (Radial PIM) [19–22], and Boundary Cloud Method (BCM) [23]. Most of the meshless methods use approximation functions along the lines of the Moving Least Squares Method [24] and of the EFGM.

The present work is an extension of the hp-Cloud Method in order to apply it to the Boundary Element Method, following the path presented in [25].

Hp-Cloud approximations have been proved to be more efficient than those of the EFGM, [9], [26], and for this reason they were used in [25]. Later, Oden, Duarte and

* Corresponding author. Fax: +55 48 331 9277.
E-mail addresses: lauro@grante.ufsc.br (L.C. Nicolazzi), clovis@pucminas.br (C.S. Barcellos), fancello@grante.ufsc.br (E.A. Fancello), armando.duarte@ualberta.ca (C.A.M. Duarte).

0955-7997/$ - see front matter © 2005 Elsevier Ltd. All rights reserved.
doi:10.1016/j.enganabound.2004.12.003

Zienkiewicz, [10], proposed that, instead of using circles or rectangles for defining the Clouds around each node, it would be more convenient to use linear finite element meshes. Here the Clouds associated to node '*i*' would be built by the union of the 'elements' connected to this node. This concept greatly reduces the number of floating point operations, since the Partition of Unity is known beforehand and allows standard integration routines for integrating the nodal matrices. This new scheme led to the Generalized Finite Element Method, GFEM.

In this paper, some choices of Partition of Unity are discussed and one of them is selected to be applied to the Galerkin Boundary Element Method. This Partition of Unity is then enriched by a set of functions like polynomials of equal or unequal degrees in different directions, particular solutions, or other reasonable functions to span the approximation space. A choice of error indicators in order to adaptively enrich the Partition of Unity is here described. This new technique is hereafter called the Generalized Galerkin Boundary Element Method (GGBEM). The L-shaped domain and the Motz potential problems are solved by the Classic (singular), Hyper and Symmetric methods and their results for both uniform and adaptive enrichment are compared and discussed.

The remainder of this paper is outlined as follows: Section 2 summarizes the Galerkin boundary integral equations for potential 2D problems; Section 3 describes the main topics of the Moving Least Squares Method, MLSM; Section 4 presents the hp-Cloud Partition of Unity functions and their enrichment is described in Sections 5 and 6 discusses some of the possible MLSM weighting functions and one in particular which leads to the generalized formulations; Section 7 presents an error indicator for the Galerkin boundary integral equations; Section 8 summarizes the selected integration and regularization procedures; Section 9 presents results of the proposed formulation for the L-shaped domain and the Motz potential problems; and the conclusions are given in Section 10.

2. Galerkin boundary elements

Since this work is mainly focused on the numerical characteristics of the approximation method, a simple differential equation in two dimensions is dealt with here.

Let us define a domain $\Omega \subset \Re^2$ by a Lipschitz boundary $\Gamma = \Gamma_{\mathscr{D}} \cap \Gamma_{\mathscr{N}}$, where the Dirichlet, $\Gamma_{\mathscr{D}}$, and Neumann, $\Gamma_{\mathscr{N}}$, parts of the boundary have null intersection, $\Gamma_{\mathscr{D}} \cap \Gamma_{\mathscr{N}} =$. Equilibrium is stated by the Laplace equation with Dirichlet and Neumann boundary conditions

$$-\Delta T(\mathbf{x}) = 0 \text{ on } \Omega, \quad T(\mathbf{x}) = f \text{ on } \Gamma_{\mathscr{D}}, \qquad \frac{\partial T}{\partial n} = g \text{ on } \Gamma_{\mathscr{N}}, \tag{1}$$

where by T we denote the unknown potential field and by $\partial T/\partial n$ its normal derivative.

The Galerkin or Variational approach in boundary integral equations [27] is given by

$$c_1 \int_\Gamma \varphi_j(d)\varphi_k(d)\mathrm{d}\Gamma(d) T_j = \int_\Gamma \int_\Gamma G(\mathbf{x},\mathbf{d})\varphi_i(\mathbf{x})\varphi_k(\mathbf{d})\mathrm{d}\Gamma(\mathbf{x})\mathrm{d}\Gamma(\mathbf{d}) \frac{\partial T_i}{\partial n} - \int_\Gamma \int_\Gamma \frac{\partial G(\mathbf{x},\mathbf{d})}{\partial n(\mathbf{x})} \varphi_i(\mathbf{x})\varphi_k(\mathbf{d})\mathrm{d}\Gamma(\mathbf{x})\mathrm{d}\Gamma(\mathbf{d}) T_i \tag{2}$$

and also by an analogous expression for the normal derivative,

$$c_2 \int_\Gamma \varphi_j(\mathbf{d})\varphi_k(\mathbf{d})\mathrm{d}\Gamma(\mathbf{d}) \frac{\partial T_j}{\partial n} = \int_\Gamma \int_\Gamma \frac{\partial G(\mathbf{d},\mathbf{x})}{\partial n(\mathbf{d})} \varphi_i(\mathbf{x})\varphi_k(\mathbf{d})\mathrm{d}\Gamma(x)\mathrm{d}\Gamma(\mathbf{d}) \frac{\partial T_i}{\partial n} - \int_\Gamma \int_\Gamma \frac{\partial^2 G(\mathbf{d},\mathbf{x})}{\partial n(\mathbf{d})\partial n(\mathbf{x})} \varphi_i(\mathbf{x})\varphi_k(\mathbf{d})\mathrm{d}\Gamma(\mathbf{x})\mathrm{d}\Gamma(\mathbf{d}) T_i \tag{3}$$

In these expressions, φ_s are the test and trial functions, c_1 and c_2 are constants determined from the *Jump Term,* $\mathbf{d}$ and $\mathbf{x}$ are the source and field point locations and G is a fundamental solution. The set of algebraic equations obtained from expression (2) is the starting point of the classical Galerkin approach. When Eq. (3) is used, an alternative set of equations is obtained, usually called the Hypersingular Galerkin approach. The Symmetric Galerkin approximation results from a choice of equations from both previous sets. In this work these approaches are, respectively, denoted by *Classic*, *Hyper* and *Symmetric*. The characteristics of the approximation space as well as the methodology of construction of the approximation functions is the focus of the next section.

3. The moving least squares method applied to the cloud method

The Moving Least Square Method (MLS) [24], is a generalization of the conventional Least Squares Method and has the important property of allowing us to weight, in different forms, the information at arbitrarily placed points in the domain. The next paragraphs present a brief description of the method.

Let a body occupying a domain $\Omega \in \Re^n$, $n=1$, 2, or 3,with contour Γ, and let f_α, $\alpha = 0,1,2,3,\ldots N$, be

the known values of a function $f(\mathbf{x})$ on an arbitrary set of N points $\mathbf{x}_\alpha \in \Omega$:

$$f_\alpha = f(\mathbf{x}_\alpha). \tag{4}$$

The main idea is to build an approximation function $u_\mathbf{y}(\mathbf{x})$ of $f(\mathbf{x})$ at a point $\mathbf{y}$ in such a way that $u_\mathbf{y}(\mathbf{x})$ essentially depends on the neighboring values f_α. To this end we define a functional $E_\mathbf{y}(u_\mathbf{y})$ weighted by the functions $\mathcal{W}_\alpha(\mathbf{y})$ in the following form

$$E_\mathbf{y}(u_\mathbf{y}) = \frac{1}{2}\sum_{\alpha=0}^{N} \mathcal{W}_\alpha(\mathbf{y})[u_\mathbf{y}(\mathbf{x}_\alpha) - f_\alpha]^2, \tag{5}$$

where $\mathcal{W}_\alpha(\mathbf{y}) : \Re^n \to \Re$ are non negative functions with monotonic decreasing values with respect to the radius $\|\mathbf{y} - \backslash\mathbf{x}_\alpha\|$. These functions belong to the space W defined by

$$W = \{\mathcal{W}_\alpha(y) \in C_0^s(\omega_\alpha), \quad s \geq 0 \\ : \mathcal{W}_\alpha(y) \geq 0, \quad \forall\, y \in \Re^n\}. \tag{6}$$

The supports ω_α of the weighting functions $\mathcal{W}_\alpha(\mathbf{y})$ are open balls with radius h_α and center in $\mathbf{x}_\alpha$, i.e.

$$\omega_\alpha = \{\mathbf{x} \in \mathfrak{r}^n : ||\mathbf{x} - \mathbf{x}_\alpha||_{\mathfrak{r}^n} \leq h_\alpha\}. \tag{7}$$

The approximation $u_\mathbf{y}(\mathbf{x})$ is constructed, from many alternatives, as a linear combination of polynomials:

$$u_\mathbf{y}(\mathbf{x}) = \sum_{j=0}^{m} a_j P_j(\mathbf{x}). \tag{8}$$

The $P_j(\mathbf{x})$ functions are components of a complete base $\mathbf{P}$ of polynomials of order $m \leq N$,

$$\mathbf{P} = \{P_0(\mathbf{x}), P_1(\mathbf{x}), \ldots, P_j(\mathbf{x}), \ldots, P_m(\mathbf{x})\} \tag{9}$$

having the following properties:

$$\mathbf{P} = \{P_i : \mathfrak{r}^n \to \mathfrak{r}, \quad P_i \in C^l(\Omega) l \geq 0, \\ i = 0, 1, \ldots, m\}. \tag{10}$$

The minimization of the functional given by the Eq. (5) with respect to the generalized coordinates results in a system of $m+1$ equations, allowing the determination of the parameters a_i such that:

$$u_\mathbf{y}(\mathbf{x}) = \sum_{j=0}^{m} a_j(\mathbf{y}) P_j(\mathbf{x}). \tag{11}$$

This procedure can be understood as a local approximation $u_\mathbf{y}(\mathbf{x})$ of function f at the point $\mathbf{y}$. In the traditional Least Squares Method, the weight $\mathcal{W}_\alpha(\mathbf{y})$ is constant, while in the MLS the coordinates a_j depend on the local point $\mathbf{y}$.

In order to clarify the MLS procedure, it is convenient to define the following arrays:

$$\mathbf{V} = \begin{bmatrix} P_0(\mathbf{x}_0) & P_1(\mathbf{x}_0) & \cdots & P_m(\mathbf{x}_0) \\ P_0(\mathbf{x}_1) & P_1(\mathbf{x}_1) & \cdots & P_m(\mathbf{x}_1) \\ \vdots & \vdots & \cdots & \vdots \\ P_0(\mathbf{x}_N) & P_1(\mathbf{x}_N) & \cdots & P_m(\mathbf{x}_N) \end{bmatrix}, \tag{12}$$

$$\tilde{\mathcal{W}}(\mathbf{y}) = \begin{bmatrix} \mathcal{W}_0(\mathbf{y}) & 0 & \cdots & 0 \\ 0 & \mathcal{W}_1(\mathbf{y}) & \cdots & 0 \\ \vdots & \vdots & \cdots & \vdots \\ 0 & 0 & \cdots & \mathcal{W}_N(\mathbf{y}) \end{bmatrix}, \tag{13}$$

$$\mathbf{a}(\mathbf{y}) = \begin{bmatrix} a_0(\mathbf{y}) \\ a_1(\mathbf{y}) \\ \vdots \\ a_m(\mathbf{y}) \end{bmatrix} \text{ and } \mathbf{f} = \begin{bmatrix} f_0 \\ f_1 \\ \vdots \\ f_N \end{bmatrix}. \tag{14}$$

With this notation, the local approximation $u_\mathbf{y}(\mathbf{x})$ and the functional $E_\mathbf{y}(u_\mathbf{y})$ can be rewritten as

$$u_\mathbf{y}(\mathbf{x}) = \mathbf{V}a(\mathbf{y}), \tag{15}$$

$$E_\mathbf{y}(u_\mathbf{y}) = \frac{1}{2}\tilde{\mathcal{W}}(\mathbf{y})(\mathbf{V}a(\mathbf{y}) - \mathbf{f}) \cdot (\mathbf{V}a(\mathbf{y}) - \mathbf{f}). \tag{16}$$

The minimum value of this functional must be achieved by a function satisfying the following first order condition:

$$\mathrm{DE}_\mathbf{y}(u_\mathbf{y})[\hat{u}] = \tilde{\mathcal{W}}(\mathbf{y})(\mathbf{V}a(\mathbf{y}) - \mathbf{f}) \cdot \mathbf{V}\hat{a} = 0, \quad \forall\, \hat{\mathbf{a}} \in \mathfrak{r}^n. \tag{17}$$

In [24] $\hat{u} = V\hat{a}$ is an arbitrary variation function. Thus, as $\hat{\mathbf{a}}$ is an arbitrary vector, the following system of equations is satisfied:

$$\mathbf{V}^T\tilde{\mathcal{W}}(\mathbf{y})\mathbf{V}a(\mathbf{y}) = \mathbf{V}^T\tilde{\mathcal{W}}(\mathbf{y})\mathbf{f}. \tag{18}$$

The solution of this system supplies the vector of parameters $\mathbf{a}$. In a more compact form, this can be written as

$$\mathbf{A}(\mathbf{y})\mathbf{a}(\mathbf{y}) = \mathbf{F}(\mathbf{y}), \text{ where } \mathbf{A}(\mathbf{y}) = \mathbf{V}^T\tilde{\mathcal{W}}(\mathbf{y})\mathbf{V} \text{ and} \\ \mathbf{F}(\mathbf{y}) = \mathbf{V}^T\tilde{\mathcal{W}}(\mathbf{y})\mathbf{f}. \tag{19}$$

The matrix $\mathbf{A}(\mathbf{y})$ must satisfy a set of minimum properties to guarantee the existence of its inverse. This subject is addressed in Section 4.2.

4. The partition of unity for boundaries

4.1. Preliminary definitions

In the Boundary Element Method the definition of an approximation space is restricted to the boundary of the domain. Thus, in this case, an adaptation of the MLS,

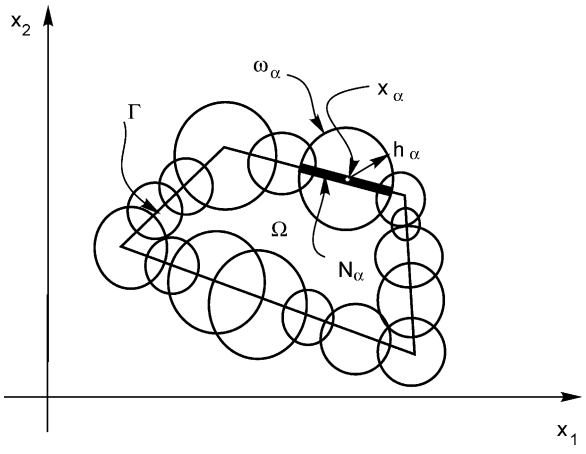

Fig. 1. Boundary cover by a set of balls.

as well as the concepts presented by Duarte and Oden [9], is necessary.

Let $\Im_N$ be a set of $N+1$ balls ω_α centered in points $\mathbf{x}_\alpha \in \Gamma$. These points are called nodes and belong to the set $Q_N = \{\mathbf{x}_0, \mathbf{x}_1, \ldots \mathbf{x}_N\} = \{\mathbf{x}_\alpha\}_{\alpha=0}^N$. The set $\Im_N$ is also associated to these nodes, as is shown in Fig. 1. It is said that $\Im_N$ is a covering of Γ if

$$\Gamma \supset \bigcup_{\alpha=0}^{N} \omega_\alpha, \omega_\alpha \in \Im_N. \tag{20}$$

Definition: A cloud η_α, shown in Fig. 1, is the intersection of the body contour with the ball ω_α, i.e.

$$\eta_\alpha := \Gamma \cap \omega_\alpha. \tag{21}$$

The set of functions $\{\varphi_\alpha\}_{\alpha=0}^N$ is called a *Partition of Unity* subordinated to the covering $\Im_N$, if they have the following properties [9]:

$$\varphi_\alpha \in C_0^\infty(\omega_\alpha) \quad 0 \le \alpha \le N, \tag{22}$$

$$\sum_{\alpha=0}^{N} \varphi_\alpha(\mathbf{x}) = 1 \quad \forall\, \mathbf{x} \in \Gamma. \tag{23}$$

A relaxation of the regularity of the functions from $C_0^\infty(\omega_\alpha)$ to $C_0^\infty(\omega_\alpha)$, $s \ge 0$, is convenient for the application of these functions in numerical methods because this allows an increase in the candidates for weighting functions $\mathcal{W}_\alpha(\mathbf{y})$.

4.2. Construction of the partition of unity

The determination of the parameters $\mathbf{a}(\mathbf{y})$ depends on the solution of the system (19) and is only possible if the matrix $\mathbf{A}$ is invertible It is possible to show that the satisfaction of this condition depends on the order of the polynomial of base $\mathbf{P}$ and the covering number of clouds η_α at each point $\mathbf{y} \in \Gamma$. A necessary condition for the existence of $\mathbf{A}^{-1}$, is that indexes $\alpha_1, \alpha_2, \ldots, \alpha_k$, $k > m$, exist, such that

$$\mathbf{y} \subset \bigcap_{j=1}^{k} \mathrm{supp}(\mathcal{W}_{\alpha_j}), \tag{24}$$

recalling that m is the maximum order of the polynomials in $\mathbf{P}$. A detailed description of this condition is discussed in Ref. [9].

Considering Eq. (19), one can write that

$$a_i(\mathbf{y}) = \sum_{j=0}^{m} \sum_{\alpha=0}^{N} \mathbf{A}_{ij}^{-1}(\mathbf{y}) P_j(\mathbf{x}_\alpha) \mathcal{W}_\alpha(\mathbf{y}) f_\alpha. \tag{25}$$

The substitution of Eq. (25) into (11) results in

$$u_{\mathbf{y}}(\mathbf{x}) = \sum_{i=0}^{m} \sum_{j=0}^{m} \sum_{\alpha=0}^{N} P_i(\mathbf{x}) \mathbf{A}_{ij}^{-1}(\mathbf{y}) P_j(\mathbf{x}_\alpha) \mathcal{W}_\alpha(\mathbf{y}) f_\alpha = \sum_{\alpha=0}^{N} \varphi_\alpha(\mathbf{x}) f_\alpha, \tag{26}$$

where

$$\varphi_\alpha(\mathbf{x}) = \sum_{i=0}^{m} \sum_{j=0}^{m} P_i(\mathbf{x}) \mathbf{A}_{ij}^{-1}(\mathbf{y}) P_j(\mathbf{x}_\alpha) \mathcal{W}_\alpha(\mathbf{y}). \tag{27}$$

It is observed that function $u_{\mathbf{y}}(\mathbf{x})$ only depends parametrically on the local point of approximation $\mathbf{y}$. Finally, if the point of approximation $\mathbf{y}$ moves together which the variable $\mathbf{x}$, that is, $\mathbf{y} = \mathbf{x}$, we have

$$u(\mathbf{x}) = u_{\mathbf{y}}(\mathbf{x}) = \sum_{\alpha=0}^{N} \varphi_\alpha(\mathbf{x}) f_\alpha, \tag{28}$$

$$\varphi_\alpha(\mathbf{x}) = \sum_{i=0}^{m} \sum_{j=0}^{m} P_i(\mathbf{x}) A_{ij}^{-1}(\mathbf{x}) P_j(\mathbf{x}_\alpha) \mathcal{W}_\alpha(\mathbf{x}). \tag{29}$$

The set of $N+1$ functions $\phi_\alpha(\mathbf{x})$ described by Eq. (29) forms a *Partition of Unity* $\{\varphi_\alpha\}_{\alpha=0}^N$. The properties of these functions, as well as the influence that the degree of the polynomials P_i exerts on the quality of approximation, are discussed below.**Lemma**. *If* $P_i \in C^n$ *and* $\mathcal{W}_\alpha \in C^s(\Gamma)$, *where* $i = 0,1,2,\ldots,m$, $\alpha = 0,1,2,\ldots,N$, $n \ge 0$, $s \ge 0$, *the set Partition of Unity,* Eq. (29), *has the property* $\{\varphi_\alpha\}_{\alpha=0}^N \in C^{\min(n,s)}(\Gamma)$.
Theorem. If $1 \in \mathbf{P}$, i.e. $\mathbf{P} = \{1, \mathrm{P}_1(\mathbf{x}), \ldots, \mathrm{P}_m(\mathbf{x})\}$, then the functions $\{\varphi_\alpha\}_{\alpha=0}^N$ *satisfy the conditions defined by* Eqs. (22) and (23). *Additionally, this base is* $\mathbf{P}$*-reducible for set* Q_N *in an explicit form*:

$$P_j(\mathbf{x}) = \sum_{\alpha=0}^{N} P_j(\mathbf{x}_\alpha) \varphi_\alpha(\mathbf{x}), \quad \forall\, \mathbf{x} \in \Gamma, \quad j = 0, 1, 2, \ldots, m. \tag{30}$$

The *Lemma* defines the regularity of the approximation functions according to the regularity of the weighting functions, $\mathcal{W}_\alpha$, as well as the degree of the approximation polynomial set $\mathbf{P}$. The *Theorem* ensures that the proposed approximation is a Partition of Unity and it is able to exactly represent any polynomial function in the subspace

generated by the set P. The proofs of the *Lemma* and the *Theorem* are found in [9].

Although the latter property is very attractive, it is possible to show that the use of polynomial functions as a basis for $\mathbf{P}$ with a higher order than zero, demands the inversion of the matrix $\mathbf{A}$, at each integration point, which greatly increases computational costs. Duarte and Oden [9] proved that the rate of convergence of the solution does not depend on the order of the polynomials of the set $\mathbf{P}$. This result leads to the selection of the simplest polynomial basis, that is

$$\mathbf{P} = \{P_0\} = \{1\}. \tag{31}$$

With this simplification, the dependence of the variable $\mathbf{y}$ in Eq. (13) disappears and the procedure for generating the *Partition of Unity* becomes easier. Moreover, the matrix $\mathbf{V}$ of Eq. (12) is reduced only to the first column with all its components equal to one. Hence, the matrix $\mathbf{A}$ and its inverse can be written as

$$\mathbf{A}(\mathbf{x}) = \mathbf{V}^{\mathrm{T}}\tilde{\mathcal{W}}(\mathbf{x})\mathbf{V} = \sum_{k=0}^{N} \mathcal{W}_k(\mathbf{x}), \tag{32}$$

$$\mathbf{A}^{-1}(\mathbf{x}) = \frac{1}{\sum_{k=0}^{N} \mathcal{W}_k(\mathbf{x})}. \tag{33}$$

Finally, the functions of the *Partition of Unity* are given by

$$\varphi_\alpha(\mathbf{x}) = \mathbf{A}^{-1}(\mathbf{x})\mathcal{W}_\alpha(\mathbf{x}) = \frac{\mathcal{W}_\alpha(\mathbf{x})}{\sum_{k=0}^{N} \mathcal{W}_k(\mathbf{x})}. \tag{34}$$

This *Partition of Unity* is known as the Shepard's scheme [24], and is used in this work.

5. Enrichment of the approximation functions

The aim of adaptive procedures is to improve the quality of the numerical results by means of adequate enrichment of the basis of approximation subspace. An efficient alternative for enriching the *Partition of Unity* consists of multiplying these functions by other ones such as polynomials, harmonic functions or even functions that are part of the solution of the boundary value problem.

This procedure generates the $\mathcal{F}_N^{k,p}$ family of functions schematically shown in the following expression:

$$\mathcal{F}_N^{k,p} = \begin{Bmatrix} \varphi_0^k Ls_0 & \varphi_1^k Ls_0 & \cdots & \varphi_N^k Ls_0 \\ \varphi_0^k Ls_1 & \varphi_1^k Ls_1 & \cdots & \varphi_N^k Ls_0 \\ \vdots & \vdots & \cdots & \vdots \\ \varphi_0^k Ls_M & \varphi_1^k Ls_M & \cdots & \varphi_N^k Ls_M \end{Bmatrix} \tag{35}$$

In this expression, N is the cloud number, index k specifies the degree of the highest polynomial order of the base $\mathbf{P}=\{P_0,P_1,\ldots,P_m\}$ and p is the dimension of the highest complete polynomial space spanned by $\mathcal{F}_N^{k,p}$. For example, let LS_T, $T=0,1,2,\ldots,M$, be the family generated for the combination of all the terms of the tensor product in $\Re^3$ of the Legendre polynomials:

$$Ls_T = L_i(x_1)L_j(x_2)L_l(x_3), \quad 0 \le i,j,l \le p, \tag{36}$$

where L_m is a polynomial of degree m in $\Re$ and $T=p=i+j+l$. For the unidimensional case, the enrichment Ls_T, is here given by the set of Legendre polynomials:

$$Ls = \{L_0, L_1, \ldots, L_p\} \tag{37}$$

and the set $\mathcal{F}_N^{k,p}$ is a space formally defined as

$$\mathcal{F}_N^{k,p} = \{\{\varphi_\alpha^k(x)\} \cup \{\varphi_\alpha^k(x)Li(x)\} : 0 \le \alpha \le N; \quad 0 \le i \le p, \quad p \ge k\}. \tag{38}$$

If the elements of the *Partition of Unity* and the enrichment family are linearly independent, so are the elements of the set $\mathcal{F}_N^{k,p}$. This property is demonstrated in Ref. [9].

If the Shepard's functions are used, the set $\mathcal{F}_N^{k,p}$ leads to

$$\mathcal{F}_N^{k=0,p=0} = \{\varphi_\alpha\}_{\alpha=0}^N \tag{39}$$

which, when enriched for the full set $\Pi_p(\Re^n)$ of polynomials, is hereafter denoted by

$$\mathcal{F}_N^{p} = \{\varphi_\alpha\}_{\alpha=0}^N. \tag{40}$$

It is important to point out that other sets of functions, different from Legendre polynomials, such as arbitrary polynomials, generalized harmonic functions, anisotropic functions as well as singular solutions of the specific problem to be analyzed, can be used for enrichment purposes.

6. Weighting functions

6.1. The choice of the weighting functions

In this subsection, the weighting function $\mathcal{W}_\alpha$ is selected in order to satisfy some conditions One of them is ease of analytical integration, since semi-analytical procedures are used in this work for integrating singular terms. Another condition is the ability to represent the solution to the differential equation. The Partition of Unity should at least be able to describe a constant function. The characteristics of the weighting functions $\mathcal{W}_\alpha$ have a great influence on the approximation process. Therefore, some conditions should be satisfied. Firstly, they should allow analytical integration, since this procedure is used here for dealing with singular terms. Secondly, they must be able to represent at least the constant function accurately.

Lancaster and Šalkauskas [24], consider some functions like the following generalized expressions:

$$\mathcal{W}_\alpha(\mathbf{x}) = \frac{s}{||\mathbf{x}-\mathbf{x}_\alpha||^\theta e^{K\rho||\mathbf{x}-\mathbf{x}_\alpha||^\beta}} \tag{41}$$

and

$$\mathcal{W}_\alpha(\mathbf{x}) = \begin{cases} \dfrac{s}{||\mathbf{x}-\mathbf{x}_\alpha||^\theta}\left\{1-\dfrac{||\mathbf{x}-\mathbf{x}_\alpha||}{h_\alpha}\right\}^\beta & \text{if } ||\mathbf{x}-\mathbf{x}_\alpha|| < h_\alpha \\ 0 & \text{if } ||\mathbf{x}-\mathbf{x}_\alpha|| \geq h_\alpha \end{cases}. \tag{42}$$

where s and K are real positive constants, θ and β are integer numbers equal to or greater than zero and h_α is the radius of the α-th ball.

Duarte and Oden [9], implemented the following weighting functions

$$\mathcal{W}_\alpha(\mathbf{x}) = \begin{cases} \sqrt{4/\pi}\left\{1-\frac{||\mathbf{x}-\mathbf{x}_\alpha||^2}{h_\alpha^2}\right\}^4 \\ \quad = k\left\{1-\frac{||\mathbf{x}-\mathbf{x}_\alpha||^2}{h_\alpha^2}\right\}^4 & \text{if } ||\mathbf{x}-\mathbf{x}_\alpha|| < h_\alpha \\ 0 & \text{if } ||\mathbf{x}-\mathbf{x}_\alpha|| \geq h_\alpha \end{cases} \tag{43}$$

and

$$\mathcal{W}(z_\alpha) = \begin{cases} \dfrac{C}{h_\alpha^n}\left[1-\dfrac{3}{2}z_\alpha^2+\dfrac{3}{4}z_\alpha^3\right] & \text{if } 0 \leq z_\alpha \leq 1 \\ \dfrac{C^\alpha}{4h_\alpha^n}[2-z_\alpha]^3 & \text{if } 1 \leq z_\alpha \leq 2 \\ 0 & \text{if } 2 \leq z_\alpha; \end{cases} \quad ; \quad z_\alpha = \frac{2}{h_\alpha}||\mathbf{x}-\mathbf{x}_\alpha||_{\Re^n} \tag{44}$$

where n is the dimension of the problem and C is a constant that depends on n. Babuška and Melenk [29] used the function of linear finite elements

$$\mathcal{W}(z_\alpha) = \begin{cases} |\mathbf{x}-\mathbf{x}_\alpha| & \text{if } \mathbf{x} \in \omega_\alpha \\ 0 & \text{if } \mathbf{x} \notin \omega_\alpha \end{cases}. \tag{45}$$

The singular weighting functions given by the Eqs. (41) and (42) are not considered in this work because they increase the degree of singularity of the strong and the hypersingular kernels.

Although weighting function (43) presents good regularity properties, it is not selected because of difficulties in analytical integration of irrational terms. In Ref. [25], Nicolazzi et al. consider a variation of Eq. (43). This latter equation, as well as Eq. (41), also presents difficulties in performing analytical integration of irrational terms.

An investigation into the influence of the weighting function properties on the Timoshenko Beam Problem is shown in [28]. The main conclusions are the following:

- the rate of convergence in p-enrichment increases with the reduction in the order of the weighting function;
- the over-covering does not improve the convergence rate;
- the over-covering increases the cost of the calculation of the partition of unity;

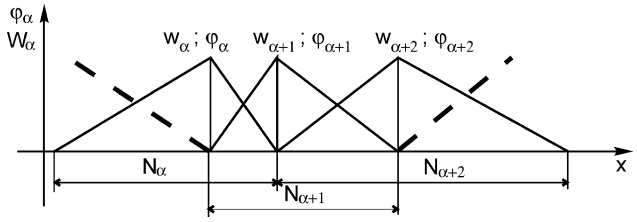

Fig. 2. The adopted partition of unity: linear tent function.

- the condition number increases more slowly for the weighting functions of lower orders in p-enrichment.

Taking these conclusions into consideration and due to the ease of integration, the linear tent function (45), shown in Fig. 2, was adopted. Therefore, the suggested enrichment scheme parallels the Generalized Finite Element Method. This scheme was independently proposed by Babuška and Melenk [29] and by Oden, Duarte and Zienkiewicz [10]. In the latter work an arbitrary domain mesh is used to define a cloud as unions of elements connected to a node, i.e. the mesh composed of linear finite elements is used to define the Partition of Unity and the cloud contours.

In cases where clouds n_α are constructed to keep a fixed covering at each point $\mathbf{x} \in \Gamma$, the resulting connectivity is the same as that in the classic boundary element method. Moreover, the tent function applied in the Shepard's scheme (34) results in a partition of unity, also shown in Fig. 2 and the classical linear elements of the Boundary Element Method are reached.

The main difference between the present method and the conventional BEM is the possibility to adaptively perform h-enrichment by simple addition of nodes $\mathbf{x}_\alpha$ and its associate clouds, as well as to adaptively enhance the solution with p-enrichment with the construction of the $\mathcal{F}_N^p$ family.

Figs. 3 and 4 show the family $\mathcal{F}_N^3$ constructed from two different *Partitions of Unity* ϕ_α, in which the vertexes of the tent are located in $x=0$ and $x=0.8$.

In this case, L_i is the enrichment polynomial function with order $0 \leq i \leq 3$ and $\phi_\alpha L_i$ is the product of this function with the Partition of Unity. It is worth to note that, in this example, the Legendre enrichment functions were scaled in

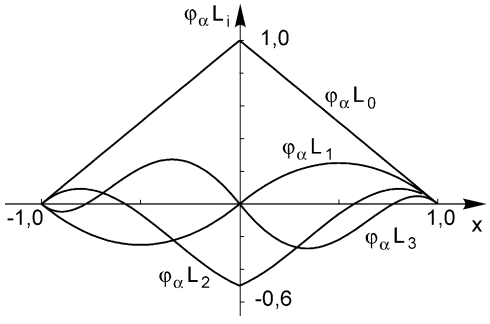

Fig. 3. The symmetric tent enriched by Legendre's polinomials up degree 3.

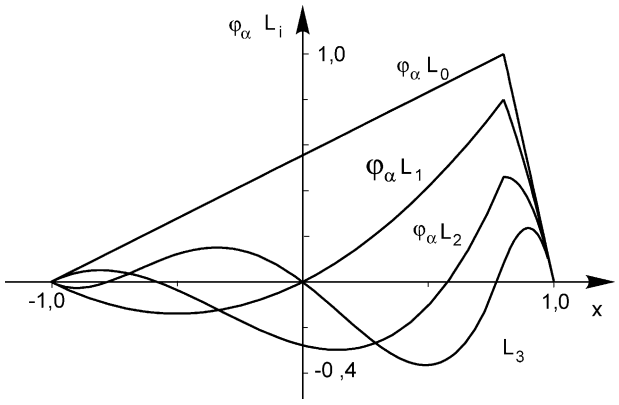

Fig. 4. The non-symmetric tent enriched by Legendre's polinomials up degree 3.

order to fit the tent support. However, other procedures may be used.

It is convenient to point out that the enriched approximation functions also belong to the set $C_0^0(\omega_\alpha)$ as can be noted in Figs. 3 and 4.

7. Error indicators

Several procedures are available to determine the sensitivity of the approximation error when a new degree of freedom is included in a *p*-adaptive methodology. This work follows the procedures stated in Oden [30–32], Duarte [33] and Jorge [34], where the residue is projected in the subspace generated by the enrichment functions.

Different expressions of residue are obtained according to the selected approach: *Classic*, *Hyper* or *Symmetric*. In the case of the *Classic* approach, the residual on the *i*th cloud has the following form:

$$R^i_{\Gamma_{\mathcal{D}}} = \varphi_j(\mathbf{d})T_j - \int_\Gamma G(\mathbf{d},\mathbf{x})\varphi_k(\mathbf{x})\mathrm{d}\Gamma(\mathbf{x})\frac{\partial T_k}{\partial n} + \int_\Gamma \frac{\partial G(\mathbf{d},\mathbf{x})}{\partial n(\mathbf{x})}\varphi_k(\mathbf{x})\mathrm{d}\Gamma(\mathbf{x})T_k \tag{46}$$

The residual for the *Hyper* approach is:

$$R^i_{\Gamma\eta} = \varphi_j(\mathbf{d})\frac{\partial T_j}{\partial n} - \int_\Gamma \frac{\partial G(\mathbf{d},\mathbf{x})}{\partial n(\mathbf{d})}\varphi_k(\mathbf{x})\mathrm{d}\Gamma(\mathbf{x})\frac{\partial T_k}{\partial n} + \int_\Gamma \frac{\partial^2 G(\mathbf{d},\mathbf{x})}{\partial n(\mathbf{d})\partial n(\mathbf{x})}\varphi_k(\mathbf{x})\mathrm{d}\Gamma(\mathbf{x})T_k. \tag{47}$$

The residual for the *Symmetric* approach is a combination of $R^i_{\Gamma_{\mathcal{D}}}$ and $R^i_{\Gamma_\eta}$, depending on the boundary conditions. If the cloud is submitted to a Dirichlet boundary condition, then $R^i_{\Gamma_{\mathcal{D}}}$ is used. Conversely, if a Neumann boundary condition is applied, then $R^i_{\Gamma_\eta}$ is chosen.

Two new functions, ψ_1 and ψ_2, instead of only one were used, so that the variation in the residual takes into account the enrichment of both, odd and even functions.

Let the *i*th cloud be enriched by two functions $\psi_m \in \mathcal{F}^p_N$, $m=1,2$. Then the residuals given by Eqs. (46) and (47) change to:

$$\tilde{R}^i_{\Gamma_{\mathcal{D}}} = \varphi_j(\mathbf{d})T_j + \psi_m(\mathbf{d})a_m - \int_\Gamma G(\mathbf{d},\mathbf{x})\left[\varphi_k(\mathbf{x})\frac{\partial T_k}{\partial n} + \psi_m(\mathbf{x})b_m\right]\mathrm{d}\Gamma(\mathbf{x}) + \int_\Gamma \frac{\partial G(\mathbf{d},\mathbf{x})}{\partial n(\mathbf{x})}[\varphi_k(\mathbf{x})T_k + \psi_m(\mathbf{x})a_m]\mathrm{d}\Gamma(\mathbf{x}) \tag{48}$$

and

$$\tilde{R}^i_{\Gamma_\eta} = \varphi_j(\mathbf{d})\frac{\partial T_j}{\partial n} + \psi_m(\mathbf{d})b_m - \int_\Gamma \frac{\partial G(\mathbf{d},\mathbf{x})}{\partial n(\mathbf{d})}\left[\varphi_k(\mathbf{x})\frac{\partial T_k}{\partial n} + \psi_m(\mathbf{d})b_m\right]\mathrm{d}\Gamma(\mathbf{x}) + \int_\Gamma \frac{\partial^2 G(\mathbf{d},\mathbf{x})}{\partial n(\mathbf{d})\partial n(\mathbf{x})}[\varphi_k(\mathbf{x})T_k d + \psi_m(\mathbf{d})a_m]\Gamma(\mathbf{x}), \tag{49}$$

The coefficients a_m and b_m depend on the boundary condition used for the cloud. The residual is required to be orthogonal to the subspace generated by $\{\psi_1,\psi_2\} \subset \mathcal{F}^p_N$, i.e.

$$\langle \tilde{R}^i_{\Gamma_c}, \psi_m(\mathbf{d})\rangle H = \int_\Gamma \tilde{R}^i_{\Gamma_c}\psi_m(\mathbf{d})\mathrm{d}\Gamma(\mathbf{d}) = 0 \quad \forall\, \psi_m(\mathbf{d}) \in \{\psi_1,\psi_2\}, \tag{50}$$

where $m=1,2$. Sub-index $c=\mathcal{D}$ or η depending, once again, on the boundary conditions.

This orthogonalization procedure leads to

$$\begin{bmatrix} \mathbf{A} & \mathbf{B}^i \\ (\mathbf{B}^i)^T & \mathbf{D}^i \end{bmatrix}\begin{pmatrix} \hat{\mathbf{x}} \\ \hat{\mathbf{c}} \end{pmatrix} = \begin{pmatrix} \hat{\mathbf{f}} \\ \hat{\mathbf{g}}^i \end{pmatrix} \tag{51}$$

where the matrices $\mathbf{A}$, $\mathbf{B}^i$ and $\mathbf{D}^i$ and the vectors $\hat{\mathbf{x}}$, $\hat{\mathbf{c}}$ and $\hat{\mathbf{g}}^i$ have dimensions $n\times n$, $n\times 2$, 2×2, n, 2 and 2, respectively, and n is the number of degrees of freedom of the system before the inclusion of ψ_1 and ψ_2.

Since an error estimator must be computationally inexpensive, a simplification is added. We consider that the new functions ψ_1 and ψ_2 modify the solution only in the neighborhood of the enriched cloud. Thus

$$\mathbf{D}^i\hat{\mathbf{c}} \cong \hat{\mathbf{g}}^i - (\mathbf{B}^i)^T\mathbf{x}, \tag{52}$$

where $\mathbf{x}$ is the solution of the problem before the enrichment.

Eq. (52) may now be used as an error indicator. We define the number:

$$\lambda^i = D^i_{jk} c_j c_k. \tag{53}$$

If λ^i is greater than a specified value, it indicates that the ith cloud should be enriched.

A simplified and additional criterion for the error indicator is given by

$$\lambda^i_1 = D^i_{11}(c^i_1)^2, \tag{54}$$

and

$$\lambda^i_2 = D^i_{22}(c^i_1)^2. \tag{55}$$

When these equations are considered with the first criterion, Eq. (53), they allow us to determine the relative importance of each polynomial enrichment in the approximate solution. These error indicators represent a local measure of the solution variation due to the enrichment of the local base by the function ψ_m:

$$\lambda = ||u\Delta\mathbf{u}||^2_{H=L_2}$$

$$= \langle \tilde{R}^i_{\Gamma_c}(\psi_1+\psi_2), \psi_1+\psi_2\rangle_{H=L_2}, \quad \{\psi_1,\psi_2\} \subset \mathcal{F}^p_N \subset L_2.$$

These error indicators are, in essence, the same as those presented by Postell and Stephan [35] for Galerkin boundary elements. In Section 9 the performance of the proposed error estimator is evaluated.

8. Integration and regularization

The equilibrium equations in the Galerkin method are obtained by double integration along field and source coordinates In two-dimensional domains this implies a generic expression of the type

$$I = \int_{\Gamma_\eta}\int_{\Gamma_\xi} \Phi(\xi,\eta)\phi(\xi)\psi(\eta)\mathrm{d}\Gamma(\xi)\mathrm{d}\Gamma(\eta), \tag{56}$$

where ξ and η are the coordinates along the boundary Γ, $\Phi(\xi,\eta)$ is the kernel and $\phi(\xi)$, $\psi(\eta)$ are shape functions in ξ and η, respectively. The kernel may be weakly singular, strongly singular or hypersingular. The integral (56) can be performed by splitting it in two parts:

$$I = \int_{\Gamma_\eta} \Theta(\eta)\psi(\eta)\mathrm{d}\Gamma(\eta), \tag{57}$$

$$\Theta(\eta) = \int_{\Gamma_\xi} \Phi(\xi,\eta)\phi(\xi)\mathrm{d}\Gamma(\xi). \tag{58}$$

The inner integral (58) captures all eventual singularities and produces a regular kernel $\Theta(\eta)$ in Eq. (57). This last expression is integrated using standard Gauss quadrature, which is the adopted procedure for all regular kernels. If necessary, several regularization procedures to integrate (58) are available in the literature (Jorge et al. [36], Kane [27], Sladek Sladek et al. [37] and [38], Ghosh et al. [39], Telles [40] and Frangi et al. [41]). For singular and hypersingular kernels, analytical integration and numerical integration combined with the method presented by Ghosh [39] was used. Let us discriminate each case:

Weakly Singular Integrals: When logarithmic kernels are present (58), a possible integration procedure is the use of special Gauss points and weights. However, this choice is quite expensive if a great number of integration points are needed. Analytical integration is quite simple in the case of straight boundaries, which is the approach used here.

Strongly Singular Integrals: For the particular case of straight boundaries the integration of the strong singular kernels may be simplified. The vector normal to the boundary and the gradient vector of the fundamental solution are orthogonal and then,

$$\frac{\partial G(\mathbf{d},\mathbf{x})}{\partial n(\mathbf{x})} = \nabla G(\mathbf{d},\mathbf{x})\cdot n(\mathbf{x}) = 0, \tag{59}$$

$$\frac{\partial G(\mathbf{d},\mathbf{x})}{\partial n(\mathbf{d})} = \nabla G(\mathbf{d},\mathbf{x})\cdot n(\mathbf{d}) = 0. \tag{60}$$

This simplifies integration of the strongly singular terms of (2) and (3) and they can be reduced to the following general form:

$$\int_\Gamma \varphi_j(\mathbf{d})\varphi_k(\mathbf{d})\mathrm{d}\Gamma(\mathbf{d}). \tag{61}$$

Difficulties arise when two consecutive boundaries are connected at one point. In this case, conventional analytical integration of (58) followed by the standard Gauss rule for (57) may be used without any transformation or regularization of the kernels.

Hypersingular integral: Following Ghosh's proposition, the hypersingular term of the integral (3),

$$\int_{\Gamma_d}\int_{\Gamma_x} \frac{\partial^2 G(\mathbf{d},\mathbf{x})}{\partial n(\mathbf{d})\partial n(\mathbf{x})}\varphi_i(\mathbf{x})\varphi_k(\mathbf{d})\mathrm{d}\Gamma(\mathbf{x})\mathrm{d}\Gamma(\mathbf{d}) \tag{62}$$

is modified by choosing

$$H(\mathbf{d},\mathbf{x}) = -G(\mathbf{d},\mathbf{x}) = \frac{1}{2\pi}\ln||\mathbf{r}|| \tag{63}$$

satisfying the condition

$$\frac{\partial^2 G(\mathbf{d},\mathbf{x})}{\partial n(\mathbf{d})\partial n(\mathbf{x})} = \frac{\partial^2 H(\mathbf{d},\mathbf{x})}{\partial \Gamma(\mathbf{d})\partial \Gamma(\mathbf{x})}. \tag{64}$$

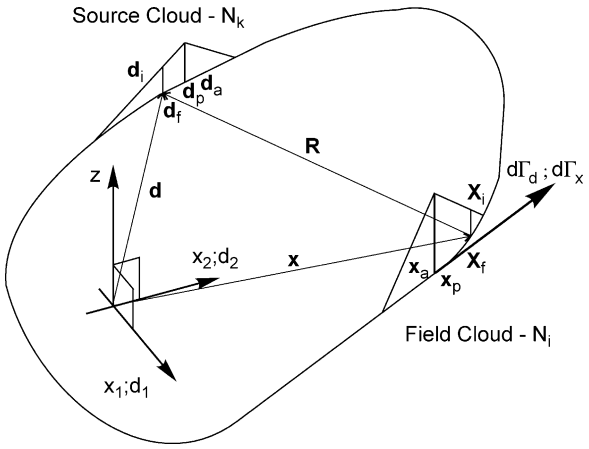

Fig. 5. The boundary and the integration path.

Hence, Eq. (62) is rewritten as

$$\int_{\Gamma_d}\int_{\Gamma_x}\frac{\partial^2 G(\mathbf{d},\mathbf{x})}{\partial n(\mathbf{d})\partial n(\mathbf{x})}\varphi_i(\mathbf{x})\varphi_k(\mathbf{d})\mathrm{d}\Gamma(\mathbf{x})\mathrm{d}\Gamma(\mathbf{d})$$

$$=\int_{\Gamma_d}\varphi_k(\mathbf{d})\left\{\int_{\Gamma_x}\frac{\partial^2 H(\mathbf{d},\mathbf{x})}{\partial\Gamma(\mathbf{d})\partial\Gamma(\mathbf{x})}\varphi_i(\mathbf{x})\mathrm{d}\Gamma(\mathbf{x})\right\}\mathrm{d}\Gamma(\mathbf{d}), \tag{65}$$

where $(\partial(\cdot)/\partial\Gamma)$ is the tangential derivative of Γ, Γ_d is the integration region the source function and Γ_x is the integration region of the field function. Finally, an integration by parts is performed in order to reduce the remaining singularity. A brief additional description will aid an understanding of the method proposed by Ghosh.

Let Ω be the domain shown in Fig. 5 closed with a boundary Γ. The integration of Eq. (65) leads to:

$$I(\mathbf{d})=\int_{\Gamma_x}\frac{\partial^2 H(\mathbf{d},\mathbf{x})}{\partial\Gamma(\mathbf{d})\partial\Gamma(\mathbf{x})}\varphi_i(\mathbf{x})\mathrm{d}\Gamma(\mathbf{x})$$

$$=\frac{\partial H(\mathbf{d},\mathbf{x})}{\partial\Gamma(\mathbf{d})}\varphi_i(\mathbf{x})\Big|_{\mathbf{x}i}^{\mathbf{x}f}-\int_{\Gamma_x}\frac{\partial H(\mathbf{d},\mathbf{x})}{\partial\Gamma(\mathbf{d})}\frac{\partial\varphi_i(\mathbf{x})}{\partial\Gamma(\mathbf{x})}\mathrm{d}\Gamma(\mathbf{x}), \tag{66}$$

where $\mathbf{x}_i$ and $\mathbf{x}_f$ are the initial and the final points of the closed boundary Γ_x. It is important to note that the kernel $(\partial H(\mathbf{d},\mathbf{x})/\partial\Gamma(\mathbf{d}))$ has a singularity of lower order than the term $(\partial^2 H(\mathbf{d},\mathbf{x})/\partial\Gamma(\mathbf{d})\partial\Gamma(\mathbf{x}))$. Substituting the integration limits, (66) is rewritten as

$$I(\mathbf{d})=\frac{\partial H(\mathbf{d},\mathbf{x}_a)}{\partial\Gamma(\mathbf{d})}\varphi_i(\mathbf{x}_a)-\frac{\partial H(\mathbf{d},\mathbf{x}_p)}{\partial\Gamma(\mathbf{d})}\varphi_i(\mathbf{x}_p)$$

$$-\int_{\Gamma_x}\frac{\partial H(\mathbf{d},\mathbf{x})}{\partial\Gamma(\mathbf{d})}\frac{\partial\varphi_i(\mathbf{x})}{\partial\Gamma(\mathbf{x})}\mathrm{d}\Gamma(\mathbf{x}). \tag{67}$$

Finally, substituting (67) in (65) and performing successive integrations, the following expression is obtained:

$$\int_{\Gamma_d}\int_{\Gamma_x}\frac{\partial^2 G(\mathbf{d},\mathbf{x})}{\partial n(\mathbf{d})\partial n(\mathbf{x})}\varphi_i(\mathbf{x})\varphi_k(\mathbf{d})\mathrm{d}\Gamma(\mathbf{x})\mathrm{d}\Gamma(\mathbf{d})$$

$$=\varphi_i(\mathbf{x}_a)\varphi_k(\mathbf{d}_a)H(\mathbf{d}_a,\mathbf{x}_a)-\varphi_i(\mathbf{x}_a)\varphi_k(\mathbf{d}_p)H(\mathbf{d}_p,\mathbf{x}_a)$$

$$-\varphi_i(\mathbf{x}_a)\int_{\Gamma_d}\frac{\partial\varphi_k(\mathbf{d})}{\partial\Gamma(\mathbf{d})}(\mathbf{d})H(\mathbf{d},\mathbf{x}_a)\mathrm{d}\Gamma(\mathbf{d})$$

$$-\varphi_i(\mathbf{x}_p)\varphi_k(\mathbf{d}_a)H(\mathbf{d}_a,\mathbf{x}_p)$$

$$+\varphi_i(\mathbf{x}_p)\varphi_k(\mathbf{d}_p)H(\mathbf{d}_p,\mathbf{x}_p) \tag{68}$$

$$+\varphi_i(\mathbf{x}_p)\int_{\Gamma_d}\frac{\partial\varphi_k(\mathbf{d})}{\partial\Gamma(\mathbf{d})}(\mathbf{d})H(\mathbf{d},\mathbf{x}_p)\mathrm{d}\Gamma(\mathbf{d})-\varphi k(\mathbf{d}_a)$$

$$\times\int_{\Gamma_d}\frac{\partial\varphi_i(\mathbf{x})}{\partial\Gamma(\mathbf{x})}H(\mathbf{d}_a,\mathbf{x})\mathrm{d}\Gamma(\mathbf{x})+\varphi_k(\mathbf{d}_p)$$

$$\times\int_{\Gamma_d}\frac{\partial\varphi_i(\mathbf{x})}{\partial\Gamma(\mathbf{x})}H(\mathbf{d}_p,\mathbf{x})\mathrm{d}\Gamma(\mathbf{x})-\int_{\Gamma_d}\int_{\Gamma_x}\frac{\partial\varphi_k(\mathbf{d})}{\partial\Gamma(\mathbf{d})}H(\mathbf{d},\mathbf{x})$$

$$\times\frac{\partial\varphi_i(\mathbf{d})}{\partial\Gamma(\mathbf{d})}\mathrm{d}\Gamma(\mathbf{x})\mathrm{d}\Gamma(\mathbf{d})$$

where $\mathbf{d}_a$, $\mathbf{x}_a$, $\mathbf{d}_p$ and $\mathbf{x}_p$ are the coordinates of the point where $\varphi_k(\mathbf{d})=\varphi_i(\mathbf{x})=1$. It must be noted that, when the clouds are not centered at the boundary vertexes, Eq. (68) is reduced to the last term only. Expression (68) contains only weakly singular kernels, which are much simpler than those of the original form (62). However, care is required for some constants of this equation as the radius $\mathbf{r}=\mathbf{d}-\mathbf{x}$, represented by $(\mathbf{d},\mathbf{x})$ is null when $\mathbf{d}_a\equiv\mathbf{x}_a$, $\mathbf{d}_p\equiv\mathbf{x}_a$, $\mathbf{d}_a\equiv\mathbf{x}_p$ or $\mathbf{d}_p\equiv\mathbf{x}_p$. To remove this singularity the technique shown in [27] is followed. It is also important to remark that in the present regularization procedure no approximation is involved.

9. Numerical results

9.1. Motz problem

In order to test the efficiency of the proposed numerical approach, a heat conduction problem with a severe discontinuity of the heat flux is analyzed The Motz problem, [42,43], consists of a rectangular domain subjected to the boundary conditions shown in Fig. 6.

The analytic solution of this problem is given by a series of harmonic functions [43]:

$$T(r,\theta)=\sum_{l=0}^{M}b_l r^{l+(1/2)}\cos\left(l+\frac{1}{2}\right)\theta, \tag{69}$$

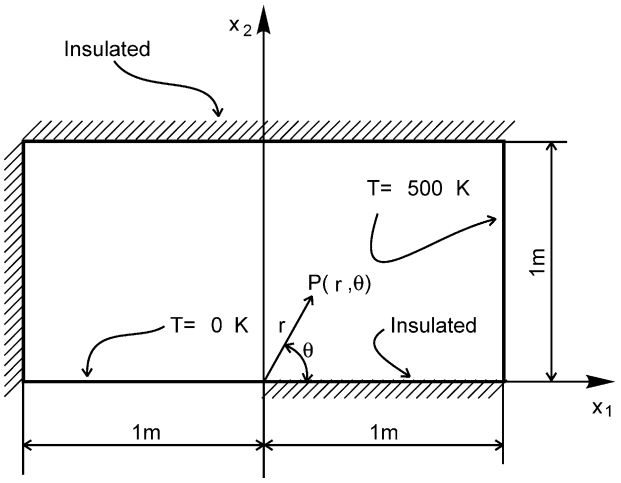

Fig. 6. The Motz problem.

where (r,θ) are the polar coordinates, b_l, $l=0,1,2,3,\ldots,M$ are the Fourier coefficients of the series. One may note that there is a singularity in the flux at $x_1=x_2=0$. The heat flux has a singular term of the type $1/\sqrt{r}$ when $r=0$ and $l=0$.

The energy norm for this problem, [42], specifically for the present data, Eq. (70), is

$$||\tilde{T}(\mathbf{x})||_E^2 = \int_{\Gamma_{\mathcal{D}}} \bar{T}(\mathbf{x})\frac{\partial \tilde{T}(\mathbf{x})}{\partial n(\mathbf{x})}\mathrm{d}\Gamma + \int_{\Gamma_n} \tilde{T}(\mathbf{x})\frac{\partial \bar{T}(\mathbf{x})}{\partial n(\mathbf{x})}\mathrm{d}\Gamma = 85079.28 \tag{70}$$

The relative error η in the energy norm ([42]) is evaluated as

$$\eta = 100\frac{\sqrt{||\tilde{T}(\mathbf{x})||_E^2 - ||T(\mathbf{x})||_E^2}}{||\tilde{T}(\mathbf{x})||_E} \tag{71}$$

where $T(\mathbf{x})$ is the numerical approximation of the temperature field. Approximate solutions are computed by using the following strategies:

1. Uniform mesh and uniform p refinement;
2. Uniform mesh and adaptive p refinement;
3. Geometrically refined mesh (factor 0.15 toward the singular point) and uniform p refinement;
4. Geometrically refined mesh and adaptive p refinement;

Numerical tests are performed with two meshes composed of 15 and 35 clouds (3 and 7 clouds on each boundary segment, respectively. See Fig. 15). The relative error (71), is plotted as a function of the *Number of Approximation Terms*, (NAF). The rate of convergence, [44], is computed as the angular coefficient of the line joining two consecutive

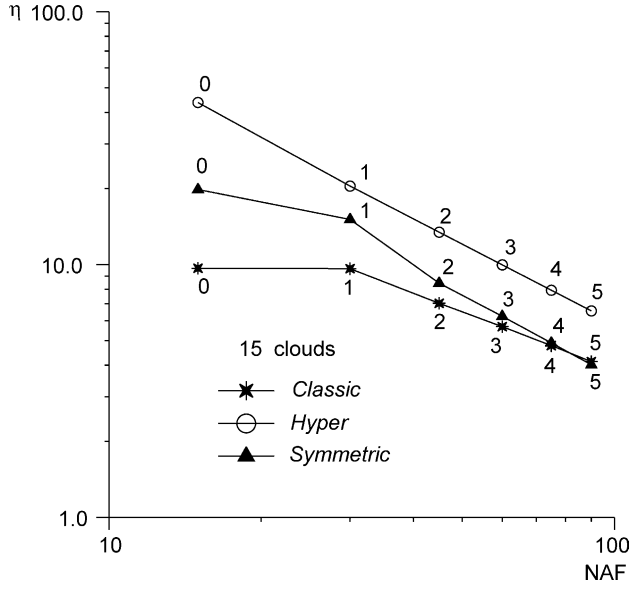

Fig. 7. Convergence for uniform mesh and uniform *p* refinement. Mesh with 15 clouds.

points on the graph $\eta\times$NAF:

$$a = \frac{\log(\eta_1/\eta_2)}{\log(\mathrm{NAF}_1/\mathrm{NAF}_2)}, \tag{72}$$

where: η_i is the error for NAF_i.

9.1.1. Strategy 1. Uniform mesh and uniform p refinement

The results for this case are displayed in Figs. 7 and 8 which show similar tendencies for the three formulations. For low *p*-order, the *Classic* formulation presents better results. However, as the enrichment proceeds, the *Symmetric* formulation shows a better performance. All three

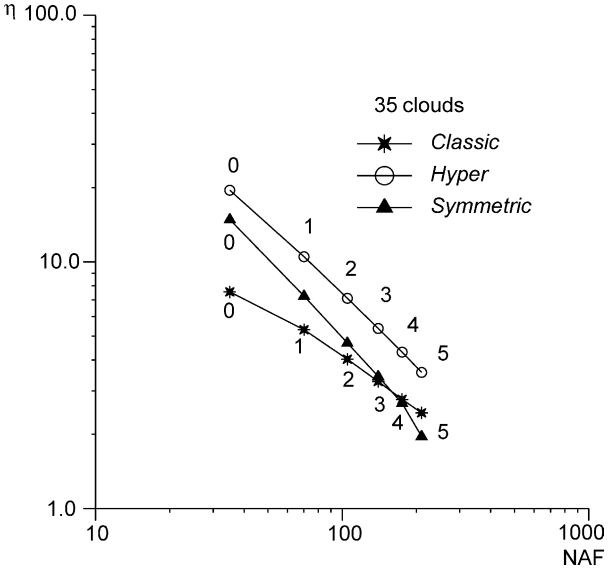

Fig. 8. Convergence for uniform mesh and uniform *p* refinement. Mesh with 35 clouds.

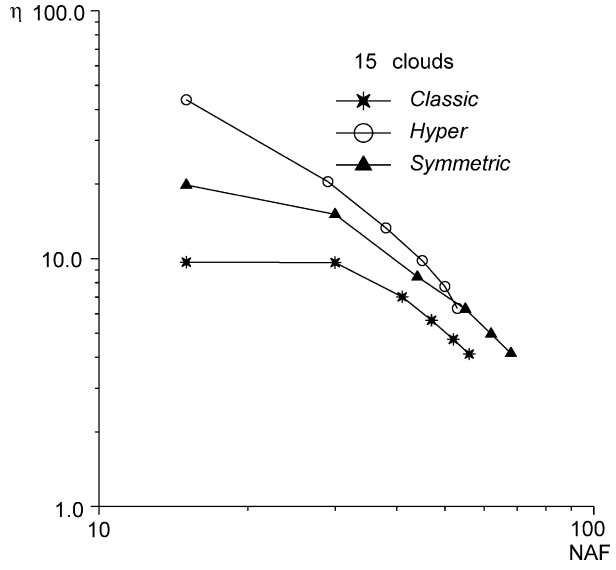

Fig. 9. Convergence for uniform mesh and adaptive p refinement. Mesh with 15 clouds.

approaches present an approximately algebraic convergence after a pre-asymptotic behavior.

9.1.2. Strategy 2. Uniform mesh and adaptive p refinement

The results for this example are presented in Figs. 9 and 10. The three formulations show a similar convergence performance for both meshes, although errors are larger for low numbers of clouds, as expected. The adaptive scheme is remarkably superior to the uniform one as can be noted in Tables 1 and 2.

9.1.3. Strategy 3. Geometric mesh and uniform p refinement

In this example, clouds of the boundaries attached to the singular point are distributed in geometric progression

Table 1
Error η for Strategy 1

Strategy 1						
Clouds	*Classic*		*Hyper*		*Symmetric*	
	NAF	η	NAF	η	NAF	η
15	90	4.1314	90	6.5583	90	4.0172
35	210	2.4399	210	3.5613	210	1.9578

Table 2
Error η for Strategy 2

Strategy 2						
Clouds	*Classic*		*Hyper*		*Symmetric*	
	NAF	η	NAF	η	NAF	η
15	56	4.1195	53	6.2952	68	4.1469
35	73	2.4832	62	3.6181	105	2.1785

with a factor 0.15 toward this point. The polynomial enrichment is uniform along all clouds. One may observe that, in this case, the *Symmetric* approach shows an oscillatory pre-asymptotic behavior when few clouds are used (Fig. 11) and more stable convergence for a refined mesh (Fig. 12). Additionally, the *Classic* and *Hyper* formulations present a pre-asymptotic phase and later converge exponentially. (Fig. 12 and Table 3).

9.1.4. Strategy 4. Geometric mesh and adaptive p refinement

In this example the influence of both, mesh and p refinements is focused. The convergence curves are presented in Figs. 13 and 14. The *Symmetric* approach

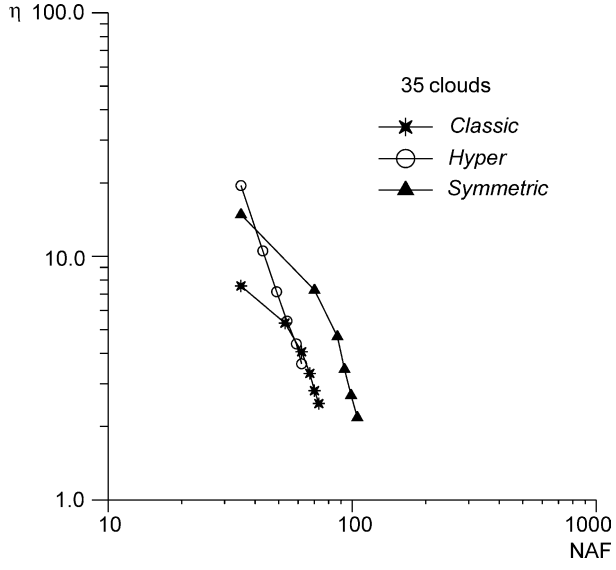

Fig. 10. Convergence for uniform mesh and adaptive p refinement. Mesh with 35 clouds.

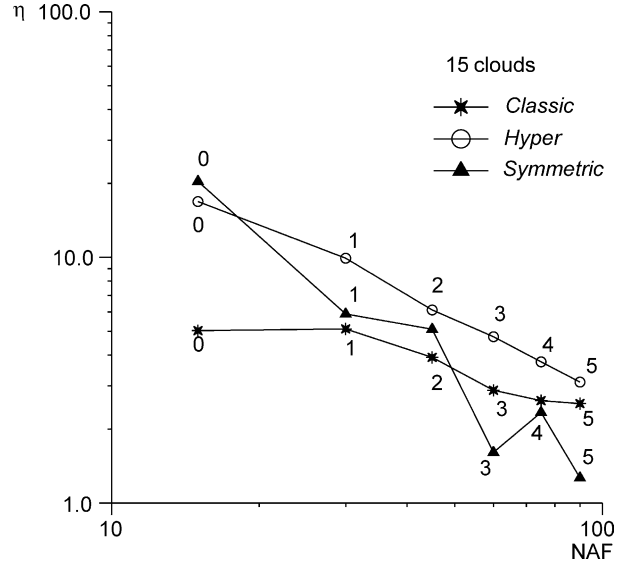

Fig. 11. Convergence for geometric mesh and uniform p refinement. Mesh with 15 clouds.

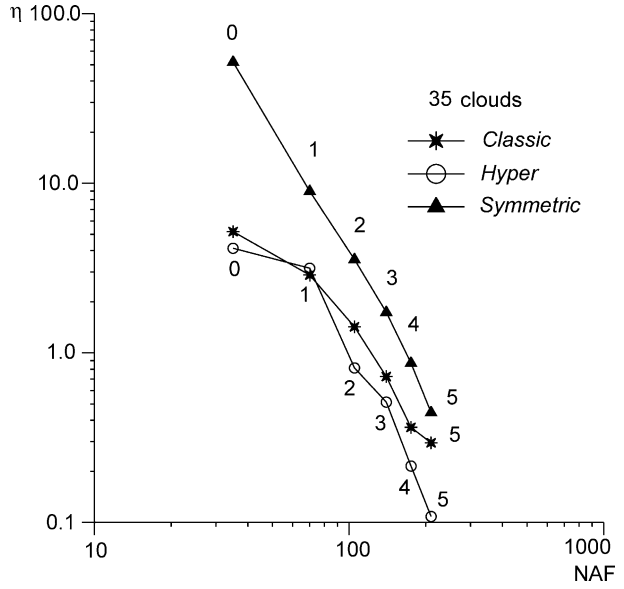

Fig. 12. Convergence for geometric mesh and uniform *p* refinement. Mesh with 35 clouds.

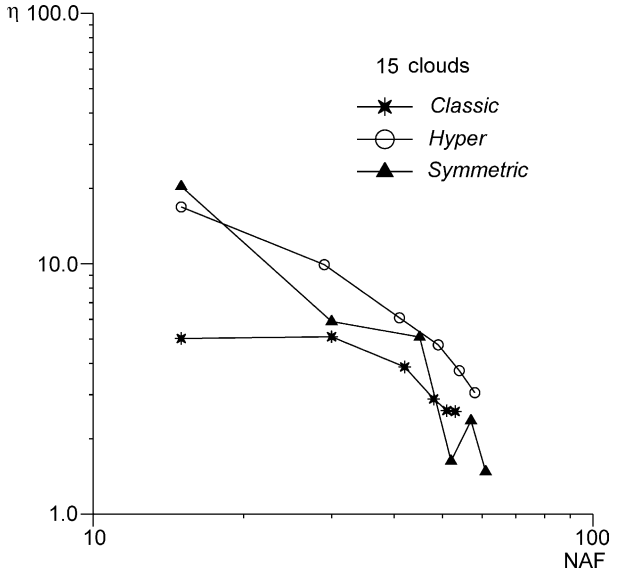

Fig. 13. Convergence for geometric mesh and uniform *p* refinement. Mesh with 15 clouds.

shows exponential behavior only for the 35-cloud mesh. *Classic* and *Hyper* approaches also show asymptotic convergence for the smallest mesh but a strong oscillation for the mesh with 35 clouds (Fig. 12). Since this doesn't occur for uniform meshes (Figs. 7 and 8) this lack of convergence seems to be associated with the very small elements close to the singular point that introduce badly conditioned matrices. This effect also seems to be less sensitive for the *Symmetric* formulation that presents a very smooth convergence curve (see Tables 3 and 4).

9.1.5. p enrichment

This section is used to analyze the polynomial distribution obtained with the fourth strategy for the mesh with 35 clouds (Fig. 15). Double nodes are used at the corners as well as at the singular point B which is shared by clouds 7 and 8. Clouds 1–7 and 14–8 are distributed geometrically toward the singular point B. The polynomial distribution along the boundary is shown in Figs. 16, 17 and 18.

The theoretical convergence for the Variational or Galerkin Boundary Element Method has been presented by a number of authors. Among them one can mention Schawatz et al. [45], Postell and Stephan [35], Stephan and Suri [46] and Yu [47]. All of them prove that the approximation error for quasi uniform meshes and *p* adaptive schemes is algebraic in Sobolev norm and can be described by expressions like

Table 3
Convergence rate for Strategy 3

Strategy 3–35 clouds						
NAF	*Classic*		*Hyper*		*Symmetric*	
	η	*a*	η	*a*	η	*a*
35	5.1820	–	4.1339	–	51.8	–
70	2.8736	0.8507	3.1530	0.3908	8.9581	2.5317
105	1.4211	1.7366	0.8146	3.3381	3.5501	2.2828
140	0.7236	2.3460	0.5119	1.6148	1.7333	2.4922
175	0.3631	3.0904	0.2149	3.8892	0.8696	3.0909
210	0.2946	1.1476	0.1083	3.7569	0.4444	3.6822

Geometric mesh, uniform *p*. 35 clouds.

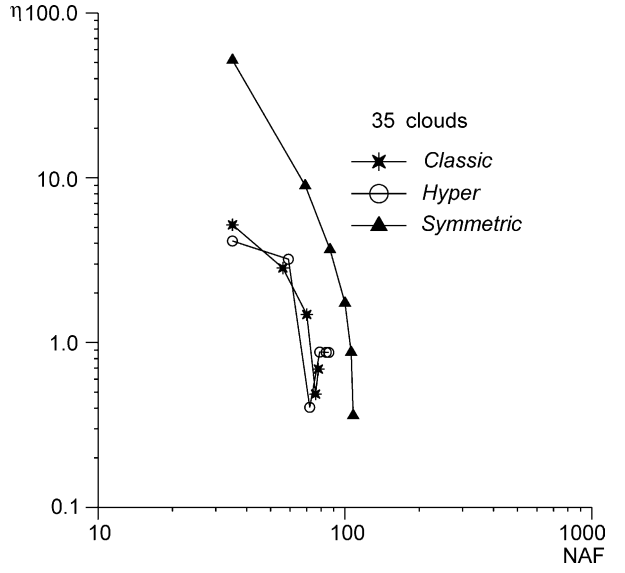

Fig. 14. Convergence for geometric mesh and adaptive *p* refinement. Mesh with 35 clouds.

Table 4
Convergence rate for Strategy 4

Strategy 4–35 clouds								
NAF	*Classic*			*Hyper*			*Symmetric*	
	η	a	NAF	η	a	NAF	η	a
35	4.8833	–	35	4.1764	–	35	51.8	–
56	2.7911	1.2849	59	3.1995	0.4888	69	8.9582	2.5853
70	1.5144	2.9127	72	0.8329	10.3948	87	3.6697	3.8501
76	0.3836	13.516	79	0.5128	−8.3314	100	1.7386	5.3643
78	0.6105	−13.427	84	0.5393	0.0661	106	0.8744	11.795
–	–	–	86	0.5370	0.0639	108	0.3608	47.351

Geometric mesh, uniform p. 35 clouds.

$$||w - w_p||_{H^\gamma} \leq Cp^{-(s-\gamma)}||w||_{H^s}, \tag{73}$$

where

$\|\cdot\|_{H^\gamma}$ stands for the Sobolev norm H^γ;
$w \in H^s(\Gamma)$ is the exact solution;
w_p is the approximate solution and belongs to the family $\mathcal{F}_N^p$;
$p = 0,1,2,3,\ldots$;
C is a constant independent of p and dependent on the boundary partition Γ and on s;
γ is related to the order of the integral operator;

Since the Sobolev and Energy norms are equivalent, [48], one may conclude that the results obtained for the *Symmetric* formulation for the first two schemes are in agreement with the theoretical predictions (Eq. (73)). The same kind of asymptotic convergence was found for the *Classic* and *Hyper* formulations. In addition, when geometric meshes are used, the convergence curve follows the a priori expression for the *hp* adaptive approaches (Postell, [35] and Babuška, [49]):

$$||e||_{H^t} \leq C^* e^{-b\sqrt{NAF}}, \tag{74}$$

where

$\|\cdot\|_H$ is the Sobolev norm H^t;
$e = \Phi - \Phi_p$ is the error;
NAF is the number of approximation functions;
C* and b are positive constants which depend on the cloud distribution but not on the NAF.

In [49] Babuška identifies the following behavior for the *hp*-FEM around a singular point: 'The true optimal meshes are geometrically graded toward the singular point with element degrees which are described by a nearly linearly increasing function starting in the second element away from the singularity. Further, the degree of the first element next to the singular point is greater than or equal to the degree of the second element'. The results for the Motz problem using the Strategy 4, as far as the rate of convergence and polynomial degrees distribution are concerned, Table 4, seem to be in agreement with the above statement. Low values of p are needed around the singular point which is conveniently characterized by the geometric mesh refinement around it.

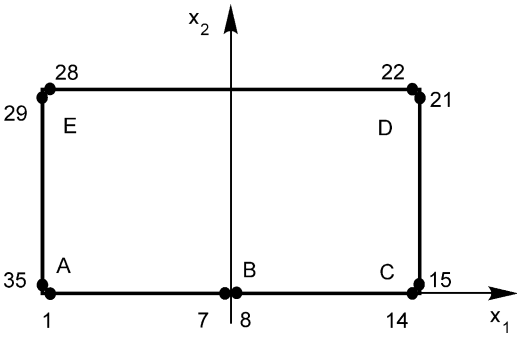

Fig. 15. Distribution of 35 clouds over the boundary.

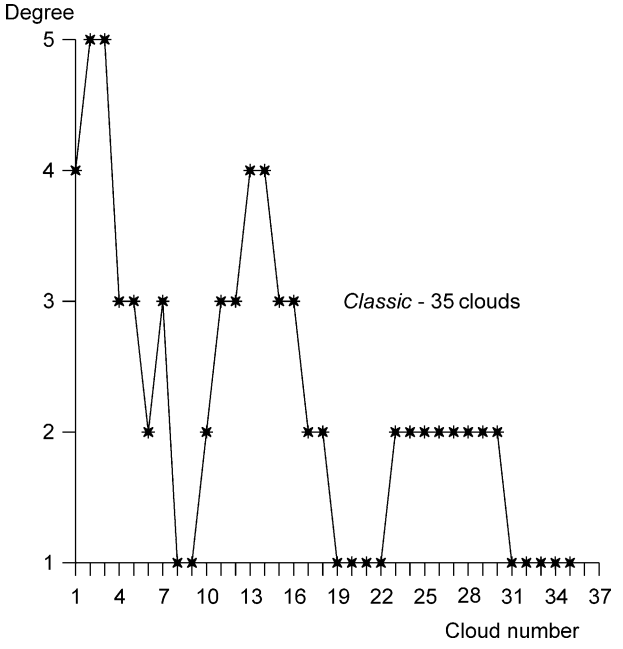

Fig. 16. Polynomial degree distribution along segment A–C. *classic formulation.*

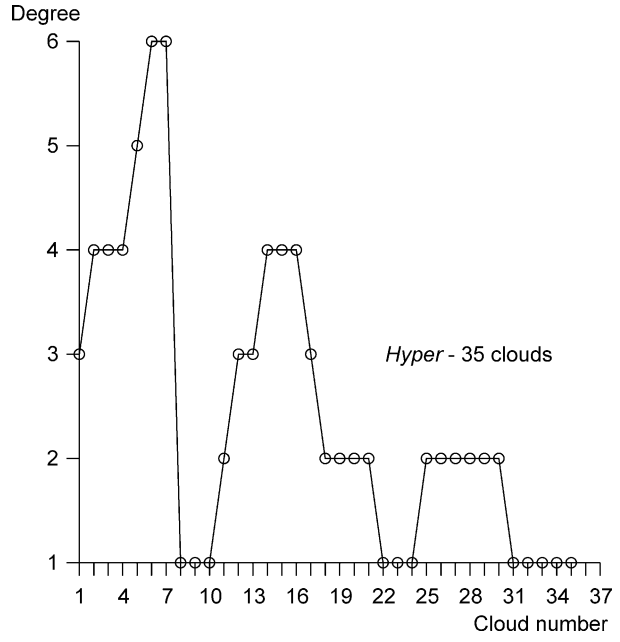

Fig. 17. Polynomial degree distribution along segment A–C. *hyper formulation.*

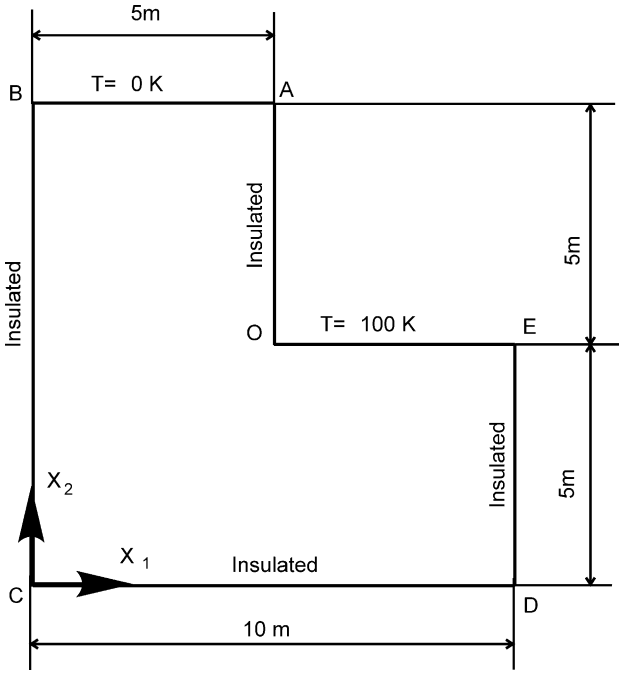

Fig. 19. L-shaped domain problem and the boundary conditions.

9.2. L-Shaped domain problem

This problem consists of the analysis of heat distribution in a *L-shaped domain.* The geometry, coordinate system and boundary conditions are shown in Fig. 19. Since this problem does not have a closed form solution, a finite element approximation is used for comparison. In this case, quadratic finite elements are used with a total of 1872 degrees of freedom. The mesh is shown in Fig. 20 having a strong refinement (but not geometric) near the singular point. Twenty clouds are uniformly distributed along edges $\bar{AB}$, $\bar{BC}$, $\bar{CD}$, and $\bar{DE}$ of Fig. 19. Edges $\bar{EO}$ and $\bar{OA}$ are covered by 26 clouds where 20 of them are equally distributed. The remaining 6 are geometrically placed within a neighborhood of 0.25 m around the singular point. The value of the geometric progression ratio is 0.15. Hence, the model has initially 132 approximation

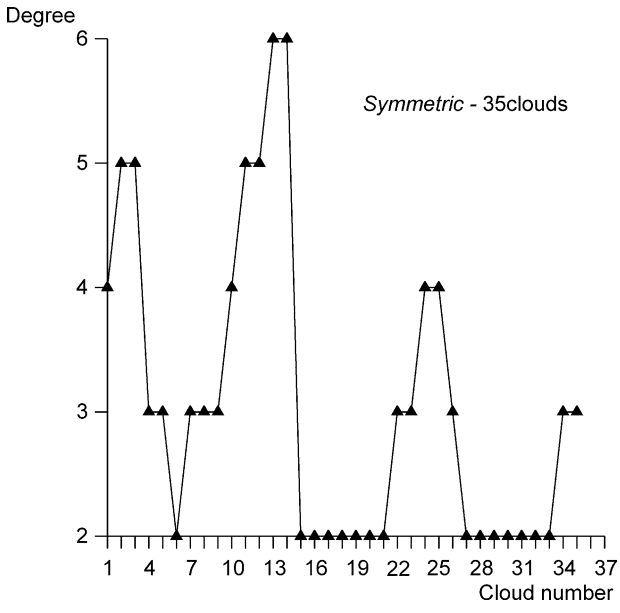

Fig. 18. Polynomial degree distribution along segment A–C. *symmetric formulation.*

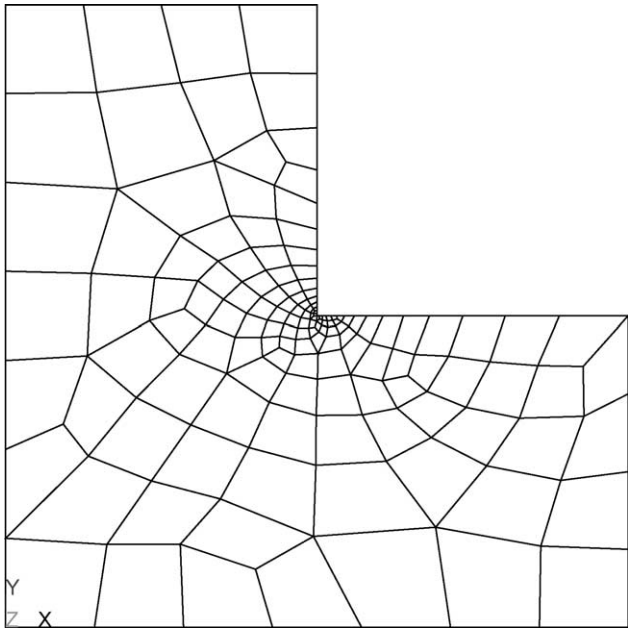

Fig. 20. Finite element model.

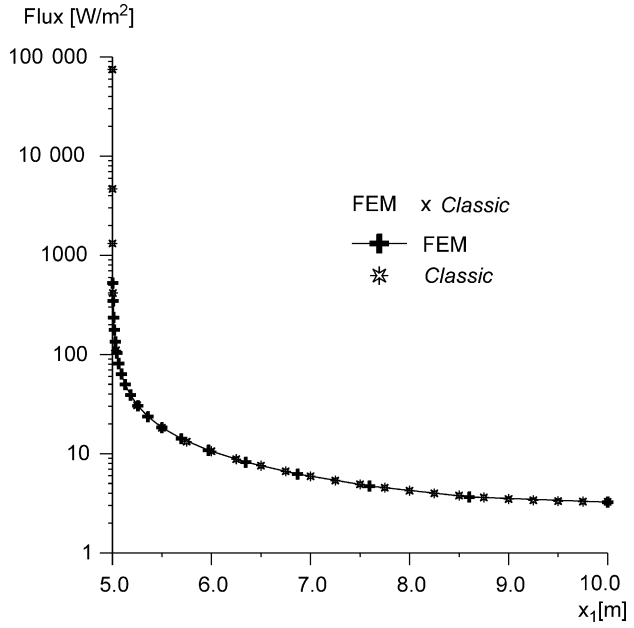

Fig. 21. GBEM-FEM solutions. *classic* formulation.

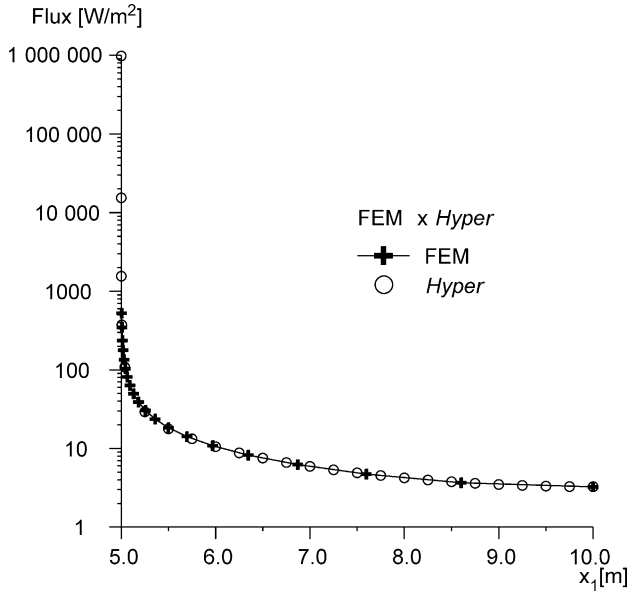

Fig. 22. GBEM-FEM solutions. *hyper* formulation.

functions, reaching 144 after *p*-enrichment for the *Classic* approach, 147 for the *Hyper*, and 167 for the *Symmetric* approach.

Figs. 21–23 illustrate a visual comparison of the three BEM formulations with the finite element solution. The results show the heat flux along the edge $\widetilde{EO}$ (Fig. 19).

An agreement between the FEM and GBEM heat flux profiles is observed even very close (0.002 m) to the singular point. For smaller distances, the chosen finite element mesh fails to represent the singularity while the GBEM, with an appropriate refinement, behaves quite well.

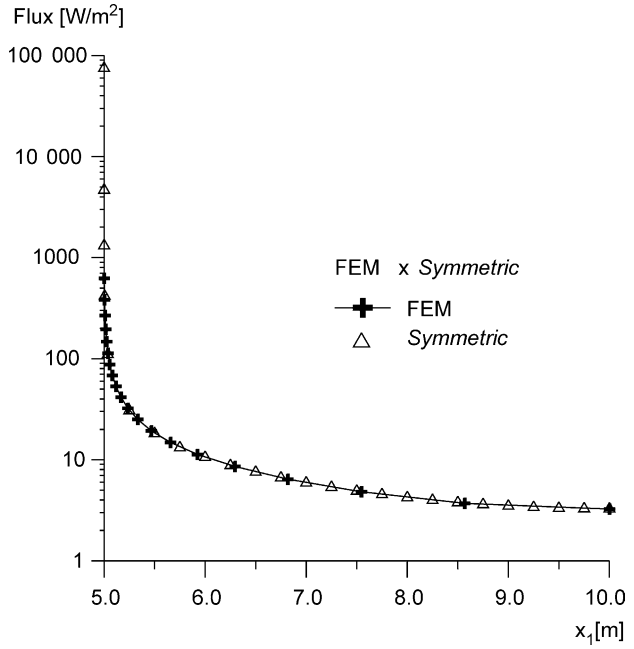

Fig. 23. GBEM-FEM solutions. *symmetric* formulation.

10. Conclusions

This paper presents a procedure that improves the advantages of the BEM for modeling different classes of physical phenomena Starting from the geometrical data given by B-Splines one may spread a set of nodes on the boundaries of the domain and automatically generate *clouds* to form an open covering of each of the boundaries. Next, it is shown how to use the Moving Least Square Method together with the clouds definition in order to obtain a partition of unity. The fundamental step of the procedure is the possibility of easily defining p-enrichment of test and trial functions locally and hierarchically. In addition, the partition of unity framework allows the enrichment with non-polynomial functions which can be very advantageous in many classes of problems, like those with singularities, discontinuities, boundary layers, etc.

An error indicator is also proposed and used to control the selective enrichment of the clouds. Numerical results show a convergence behavior in agreement with adaptive procedures. Uniform as well as geometric meshes are used in the numerical experiments. Exponential convergence is attained.

Three integral formulations are used in the numerical experiments: *Classic*, *Hyper* and *Symmetric*. Numerical experiments indicate that the *Symmetric* version is more stable and reliable for p-adaptive procedures.

References

[1] Nayroles B, Touzot G, Villon P. Generalizing the finite element method: diffuse approximation and diffuse elements. Comput Mech 1992;10:307–18.

[2] Amarantuga K, Williams JR, Qian S, Weis J. Wavelet galerkin solutions for one-dimensional partial differential equations. Int J Num Meth Eng 1994;37:2703–16.

[3] Belytschko T, Lu YY, Gu J. Crack propagation by element free galerkin methods. In advanced computational methods for material modeling, AMD-v.180/PVP-v.268, ASME (1993), pp. 191–205.

[4] Liu WK, Jun S, Zhang Y. Reproducing kernel particle methods. Int J Num Meth Eng 1995;20:1081–106.

[5] Atluri SN, Zhu T. New meshless local Petrov–Galerkin (MPLG) approach in computational mechanics. Comput Mech 1998;22: 117–27.

[6] Sukumar N, Moran B, Belytschko T. The natural element method. Int J Num Meth Eng 1998;43:839–87.

[7] Babuška I, Melenk JM. The partition of unity method. Technical note BN-1185, Institute for physical science and technology, University of Maryland, (1995).

[8] Duarte CA, Oden JT. Hp clouds—a meshless method to solve boundary value problems. TICAM Report 95-05, University of Texas, (1995).

[9] Duarte CA, Oden JT. H-p clouds-an h-p meshless method. Num Meth Partial Diff Eq 1996;1–34.

[10] Oden JT, Duarte CA, Zienkiewicz OC. A new cloud-based hp finite element method. Comput Methods Appl Mech Eng 1998;153:117–26.

[11] Duarte CA, Babuška I, Oden JT. Generalized finite element methods for the three dimensional. Struct Mech Probl Comput Struct 2000;77: 215–32.

[12] Sukumar N, Moes N, Moran N, Belytschko T. Extended finite element method for three-dimensional crack modelling. Int J Num Meth Eng 2000;48:1549–70.

[13] Mukherjee YX, Mukherjee S. The boundary node method for potential problems. Int J Num Meth Eng 1997;40:797–815.

[14] Chati MK, Mukherjee S, Paulino GH. The meshless hypersingular boundary node method for three-dimensional potential theory and linear elasticity problems. Eng Anal Boundary Elem 2001;25: 639–53.

[15] Chati MK, Mukherjee S, Paulino GH. The meshless standard and hypersingular boundary node methods—applications to error estimation and adaptivity in three-dimensional problems. Int J Numer Methods Eng 2001;50(9):2233–69.

[16] Zhu T, Zhang JD, Atluri SN. A local boundary integral equation (LBIE) method in computational mechanics, and a meshless discretization approach. Comput Mech 1998;21:223–35.

[17] Sladek J, Sladek V. Local boundary integral equation methods in solid mechanics. WCCM V. fifth world congress on computational mechanics, Austria 2002.

[18] Chen W. Meshfree boundary particle method applied to Helmholtz problems. Eng Anal Boundary Elem 2002;26:577–81.

[19] Wang JG, Liu GR. On the optimal shape parameters of radial basis functions used for 2-D meshless methods. Comput Methods Appl Mech Eng 2002;191:2611–30.

[20] Li J, Hon YC, Chen CS. Numerical comparisons of two meshless methods using radial basis functions. Eng Anal Boundary Elem 2002; 26:205–25.

[21] Mai-Duy N, Tran-Cong T. Mesh-free radial basis function network methods with domain decomposition for approximation of functions and numerical solution of Poisson's equations. Eng Anal Boundary Elem 2002;26:133–56.

[22] Li J, Hon YC, Chen CS. Numerical comparisons of two meshless methods using radial basis functions. Eng Anal Bound Elem 2002;26: 205–25.

[23] Li G, Aluru NR. A boundary cloud method with a cloud-by cloud polynomial basis. Eng Anal Bound Elem 2003;27:57–71.

[24] Lancaster P, Šalkauskas R. Curve and surface fitting, an introduction. San Diego: Academic Press; 1986.

[25] Nicolazzi LC, Duarte CA, Fancello EA, de Barcellos CS. *hp* Clouds—a meshless method in boundary elements. Part II: implementation. In: first Brazilian seminar on the boundary element method in engineering. *Anais*… Rio de Janeiro, RJ, Brazil, August 1996. Int J Boundary Elem Methods Commun 1997;8:83–5.

[26] Duarte CA, Oden JT. An h-p adaptive method using clouds. TICAM Report 96-07, University of Texas, (1996).

[27] Kane JH. Boundary element analysis in engineering continuum mechanics. USA: Prentice Hall Inc.; 1994.

[28] de Barcellos CS, Mendonça PTR, Duarte CA. Investigations on timoshenko beam problems using the HP-Cloud Meshless FEM. *In*: IV world congress on computation mechanics. *Anais*… Buenos Aires, Argentine, (1998).

[29] Babuška I, Melenk JM. The particion of unity finite element method: basic theory and applications. Comput Methods Appl Mech Eng 1996; 139(1–4):289–314.

[30] Demkowicz L, Oden JT, Rachowicz W, Hardy O. Toward a universal h-p adaptative finite element strategy, Part 1. Constrained approximation and data structure. Comput Methods Appl Mech Eng 1989;77: 79–112.

[31] Oden JT, Demkowicz L, Rachowicz W, Westermann TA. Toward a universal h-p adaptative finite element strategy, Part 2. A posteriori error estimation. Comput Methods Appl Mech Eng 1989;77:113–80.

[32] Rachowicz W, Oden JT, Demkowicz L. Toward a universal h-p adaptative finite element strategy, Part 3. Design of h-p meshes. Comput Methods Appl Mech Eng 1989;77:181–212.

[33] Duarte CAM. A Study of the p-version of finite elements for elasticity and potential problems. Brazil. Dissertação de Mestrado—UFSC. (1991). (In Portuguese).

[34] Jorge AB, Ribeiro GO, Fisher TS. Error estimators for BEM based on partial gradient recovery for higher order elements. WCCM V, fifth world congress on computational mechanics, Austria 2002.

[35] Postell FV, Stephan EP. On the h, p and hp versions of boundary element method—numerical results. Comput Methods Appl Mech Eng 1990;83:69–89.

[36] Jorge AB, Ribeiro GO, Cruse TA, Fisher TS. Self-regular boundary integral equation formulations for laplace's equation in 2-D. Int J Numer Methods Eng 2001;51:1–29.

[37] Sladek V, Sladek J. Regularization of hypersingular and nearly singular integrals in potential theory and elasticity. Int J Numer Methods Eng 1993;36:1609–28.

[38] Tanaka M, Sladek V, Sladek J. Regularization techniques applied to boundary element methods. Appl Mech Rev 1994;47(10).

[39] Ghosh N, Rajiyah H, Ghosh S, Mukherjee S. A new boundary element method formulation for linear elasticity. J Appl Mech Trans ASME 1986;53:69–76.

[40] Telles JCF. A self-adaptative co-ordinate transformation for efficient numerical evaluation of general boundary element integrals. Int J Numer Methods Eng 1987;24:959–73.

[41] Frangi A, Novati G. Symmetric BE method in two-dimensional elasticity: evaluation of double integrals for curved elements. Comput Mech 1996;19:58–68.

[42] Holzer SM. A p-Extension of the symmetric boundary element method. Comput Methods Appl Mech Eng 1993;(71):339–57.

[43] Li ZC, Manthon R, Sermer P. Boundary methods for solving elliptic problems with singularities and interfaces SIAM. J Numer Anal 1987; 24(3):487–98.

[44] Holzer SM. The h-, p- and hp- version of the BEM in elasticity: numerical results. Commun Numer Methods Eng 1995;11:255–65.

[45] Schwatz AH, Thomee V, Wendland WL. Mathematical theory of finite and boundary element methods. Germany: Birhauser Verlag Basel; 1990.

[46] Stephan EP, Suri M. On the convergence of the p-version of the boundary element galerkin method. Math Comput 1989;52(185): 1–48.

[47] De-hao Yu. Mathematical foundation of adaptative boundary element method. Comput Methods Appl Mech Eng 1991;(91): 1237–43.

[48] Kolmogorov AN, Fomin SV. Introductory real analysis. USA: Dover Publications Inc.; 1994.

[49] Babuška I, Strouboulis T, Copps K. Hp Optimization of finite element approximations: analysis of the optimal mesh sequences in one dimension. Comput Methods Appl Mech Eng 1997;150: 89–108.